



This is a repository copy of *Theoretical modelling of single-mode lasing in microcavity lasers via optical interference injection*.

White Rose Research Online URL for this paper:
<http://eprints.whiterose.ac.uk/162229/>

Version: Published Version

Article:

Wang, L-F., Wang, Y-R., Francis, H. et al. (5 more authors) (2020) Theoretical modelling of single-mode lasing in microcavity lasers via optical interference injection. *Optics Express*, 28 (11). pp. 16486-16496.

<https://doi.org/10.1364/oe.389860>

Reuse

This article is distributed under the terms of the Creative Commons Attribution (CC BY) licence. This licence allows you to distribute, remix, tweak, and build upon the work, even commercially, as long as you credit the authors for the original work. More information and the full terms of the licence here:
<https://creativecommons.org/licenses/>

Takedown

If you consider content in White Rose Research Online to be in breach of UK law, please notify us by emailing eprints@whiterose.ac.uk including the URL of the record and the reason for the withdrawal request.



eprints@whiterose.ac.uk
<https://eprints.whiterose.ac.uk/>

Theoretical Modelling of Single-Mode Lasing in Microcavity Lasers via Optical Interference Injection

LING-FANG WANG,^{1,3} YUN-RAN WANG,² HENRY FRANCIS,² RI LU,¹ MING-JUN XIA,¹ FENG LIU,¹ MARK HOPKINSON² AND CHAO-YUAN JIN^{1,2,4}

¹College of Information Science and Electronic Engineering, Zhejiang University, Hangzhou 310007, China

²Department of Electronic and Electrical Engineering, University of Sheffield, Sheffield S3 7HQ, UK

³wanglf@zju.edu.cn

⁴jincy@zju.edu.cn

Abstract: The effective manipulation of mode oscillation and competition is of fundamental importance for controlling light emission in semiconductor lasers. Here we develop a rate equation model which considers the spatially modulated gain and spontaneous emission, which are inherently governed by the ripple of the vacuum electromagnetic field in a Fabry-Pérot (FP) microcavity. By manipulating the interplay between the spatial oscillation of the vacuum field and external optical injection via dual-beam laser interference, single longitudinal mode operation is observed in a FP-type microcavity with a side mode suppression ratio exceeding 40 dB. An exploration of this extended rate equation model bridges the gap between the classical model of multimode competition in semiconductor lasers and a quantum-optics understanding of radiative processes in microcavities.

© 2020 Optical Society of America under the terms of the [OSA Open Access Publishing Agreement](#)

1. Introduction

In the rapidly developing field of photonic integrated circuits and photonic signal processing, there is a general demand for small-size and high-efficiency light sources to enable dense integration [1, 2]. Usually, a smaller laser cavity results in a larger free spectral range (FSR) and therefore a larger mode separation. However, in this case, an inhomogeneously broadened gain spectrum [3] can lead to the mode competition and effective mode manipulation can be a demanding task [4, 5]. The technical path leading to single mode operation has so far relied on the spatial modulation of the real and imaginary parts of the refractive index. A periodically modulated active region acts as an optical grating to enable wavelength selection via distributed optical feedback. For example, index-coupled distributed feedback (DFB) lasers [6], distributed Bragg reflector lasers [7], and photonic crystal lasers [8] operate on a single longitudinal mode based on a modulation of the real-part of the refractive index, whilst gain/loss modulation is successfully employed in gain-coupled DFB lasers [9-11], lasers with periodic metal structures [4] and lasers based on a pair of cavities with broken parity-time (PT) symmetry [5].

Very recently, optical interference pumping has emerged as an alternative approach to demonstrate single mode lasing in micro-sphere lasers [12, 13]. While the underlying mechanism for single mode operation is in general based on gain/loss modulation, it fundamentally differs from the previous cases, such as gain-coupled DFB lasers. In the case of gain-coupled DFB lasers, the lasing wavelength is primarily dominated by the optical grating itself, i.e. the spatial variation of the semiconductor structure, whilst the variation of the imaginary part in the refractive index breaks the PT symmetry and hence enables single mode operation [4, 5]. In the case of optical interference pumping discussed in this work, the spatial variation of the imaginary part of the refractive index determines both the lasing wavelength and the single mode operation. In addition, carrier injection is uniformly applied

in gain-coupled DFB lasers, whilst non-uniform carrier injection due to optical interference injection results in longitudinal carrier diffusion, which affects the carrier dynamics and hence increases the gain compression level. Even a small level of gain compression has a dramatic effect on the high-speed performance of lasers [14]. Therefore, a new theoretical model is needed to account for the different mechanisms described above and with which to optimise the performance of single mode lasers based on optical interference pumping.

In this work, we have developed a rate equation model to describe an FP-type microcavity laser under optical interference pumping. The conventional rate equation model is extended to further consider the interplay between the spatial variation of the vacuum electromagnetic field and the spatially modulated material gain due to optical interference pumping. Carrier diffusion amongst the pumped and unpumped regions are also included in the numerical simulation. By taking into account three longitudinal modes and varying the geometric scheme of optical interference, one of the three modes is selected to lase with a side mode suppression ratio (SMSR) exceeding 40 dB. Considering the laser dynamics, the model shows that optical interference pumping brings advantages in terms of achieving high-speed modulation in comparison with uniformly pumped lasers.

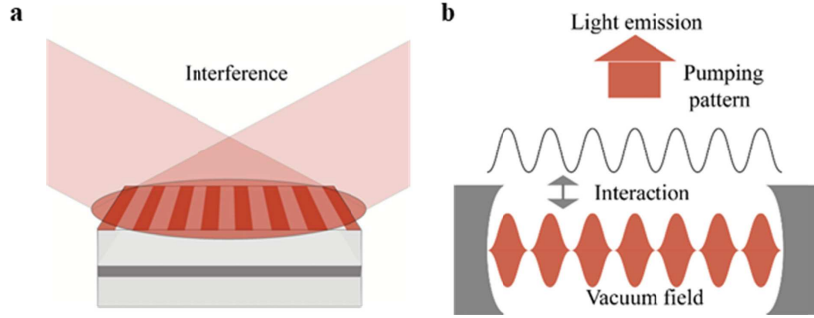


Fig. 1 Schematic images for optical interference pumping and the mode selection in an FP cavity. **a.** Dual-beam laser interference acting on the FP cavity. **b.** The interaction between the vacuum electromagnetic field of standing waves in the FP cavity and the external injection via optical interference patterning.

2. Theoretical analysis and modelling

2.1 Dual-beam laser interference

A one-dimensional theoretical model is developed to describe an FP-type microcavity laser with optical interference pumping. Fig. 1a shows the device scheme where two coherent laser beams with mirrored incident angles are applied from both sides of the FP cavity. The periodicity of the interference pattern is controlled by both the wavelength and the incident angle of the laser beams. A general form of two-beam laser interference can be considered as the superposition of electric field vectors of the beams and the intensity distribution S of a two-beam interference field can be written as:

$$S = 2A^2 - 2A^2 \cos(2kz \sin \theta), \quad (1)$$

where k is the wave number of the interference beam, A is the amplitude of the beam, θ is the incident angle, and z represents the longitudinal position [15].

Using the longitudinal mode relation in the FP cavity, $nL = m\lambda/2$, we describe the wave node of different modes, where n is the effective refractive index, L is the cavity length, and m is the number of wave nodes. Assuming the light intensity at the antinode position is A_0 , the intensity of the standing wave can be expressed as:

$$I = 2A_0 \left| \sin(nk_0 z) \right|, \quad (2)$$

where k_0 is the propagation constant corresponding to the longitudinal mode of wavelength λ . Combining formula (1) and (2), the overlap between the interference pattern and the vacuum field of standing wave can be manipulated by altering the incident angles and the wavelength of interference beams.

2.2 Travelling-wave rate equation

A travelling wave rate equation is employed to analyse the lasing properties of the spatially pumped FP cavity. The electric field in the FP cavity can be expressed as

$$E(t, z) = \left(F(t, z) e^{-ik_0 z} + R(t, z) e^{ik_0 z} \right) e^{i\omega t}, \quad (3)$$

where ω is the angular frequency, $F(t, z)$ and $R(t, z)$ represent the forward and backward optical fields in the FP cavity, respectively. The travelling-wave equation is derived from the time-dependent coupled wave equations by neglecting the coupling between the forward and backward optical fields. The fields F and R are periodically modulated using interference pumping [16-20],

$$\frac{1}{v_g} \frac{\partial F(t, z)}{\partial t} + \frac{\partial F(t, z)}{\partial z} = \left(\Gamma g(t, z) P(z) F_p - \alpha \right) F(t, z) + \frac{F_{sp}(t, z)}{L}, \quad (4)$$

$$\frac{1}{v_g} \frac{\partial R(t, z)}{\partial t} - \frac{\partial R(t, z)}{\partial z} = \left(\Gamma g(t, z) P(z) F_p - \alpha \right) R(t, z) + \frac{R_{sp}(t, z)}{L}, \quad (5)$$

where v_g is the group velocity, Γ is the confinement coefficient factor, g is the optical gain, P is the spatial factor governed by the vacuum field of standing wave, F_p is the Purcell factor, α is the internal loss, F_{sp} and R_{sp} represent the forward and reverse field of the spontaneous emission coupled into the lasing mode, and L is the length of active region. By applying the rotation wave approximation, the spatial factor of gain modulation is simplified to that of the following expression:

$$P(z) = 2 \left| \sin(nkz) \right|. \quad (6)$$

Because the periodicity of the optical interference is at the same scale as the lasing wavelength, the variation in the Purcell factor due to the spatial oscillation of the vacuum field in the FP-type microcavity should not be neglected. According to the theoretical description of the Einstein coefficients and the experiment confirmation [21-24], we take the spatially-varied Purcell enhancement into account in both the spontaneous emission and stimulated emission [25, 26]. The vacuum zero-point energy, which exists ubiquitously due to the quantization of electromagnetic fields in the resonant cavity, has the same distribution as the field of standing wave in the longitudinal direction of the cavity. Governed by Fermi's golden rule, the transition rate is proportional to the density of final states which are the vacuum states [27, 28], resulting in spatially modulated spontaneous and stimulated emission. Single-mode operation, depending on the spatial overlap between the distribution of the vacuum field and optical interference pumping, can be analysed using the above rate equations. The general mechanism for single mode operation is sketched in Fig. 1b. The Purcell factor in the discussion is defined as:

$$F_p(\lambda) = \frac{3Q}{4\pi^2 V} \left(\frac{\lambda}{n} \right)^3, \quad (7)$$

where Q is the quality factor and V is the cavity mode volume [29]. A parabolic approximation of the optical gain is used [30]

$$g(t, z, \lambda) = \frac{g_N(N(t, z) - N_0) - \left(\frac{\lambda_0 - \lambda}{G_0} \right)^2}{2(1 + \varepsilon N_p(t, z))}, \quad (8)$$

where g_N is the differential gain, N_0 is the transparent carrier density, G_0 is the parabolic gain fitting factor, and ε is the gain compression factor [31] resulted from spectral hole burning and carrier heating at high photon density. Photon density N_p is calculated by

$$N_p = \frac{\varepsilon_0 |E|^2}{h\nu}, \quad (9)$$

where ε_0 is the vacuum dielectric constant, $\varepsilon_0 |E|^2$ is the total energy of the optical field at the given frequency, ν . Considering the relationship between optical field and photon density, the forward and reverse field of the spontaneous emission coupled into the lasing mode holds as

$$F_{sp}(R_{sp}) = \sqrt{\Gamma F_p \beta \frac{N}{\tau_{sp}} \cdot \frac{L}{v_g} \cdot \frac{h\nu}{\varepsilon_0}}, \quad (10)$$

where β is the spontaneous emission factor, N is the carrier density, τ_{sp} is the spontaneous emission lifetime. The boundary conditions are given by:

$$F(0, t) = r_1 R(0, t), R(L, t) = r_2 F(L, t), \quad (11)$$

where r_1 and r_2 are the mirror reflectivity of the FP resonator's left and right facets where $r_1 = r_2$. Reducing the mirror loss increases the Q factor of the microcavity, which further increases the Purcell factor and enhances single mode oscillation via optical interference pumping.

2.3 Carrier rate equation

By taking into account the optical interference pumping and the Purcell enhancement of the spontaneous and stimulated emission, the time-dependent rate equation for the carrier densities in the active region are described by [32]

$$\begin{aligned} \frac{\partial N(t, z)}{\partial t} = & \frac{\eta_i L_{in} S}{h\nu V} - F_p \beta \frac{N(t, z)}{\tau_{sp}} - (1 - \beta) \frac{N(t, z)}{\tau_{sp}} - \frac{N(t, z)}{\tau_{nr}} \\ & - v_g 2g(t, z, \lambda) P(z) F_p N_p(t, z) + D \nabla^2 N(t, z), \end{aligned} \quad (12)$$

where η_i is the internal efficiency, L_{in} is the injected light power, $h\nu$ is the photon energy, V is the volume of active region, τ_{nr} is the non-radiative lifetime, and D is carrier diffusion coefficient [33, 34]. The value of S is 1 while using the uniform optical pumping, and S is governed by formula (1) with optical interference pumping.

2.4 Multi-mode rate equations

The longitudinal mode competition is governed by the following multimode rate equations [35, 36]

$$\left\{ \begin{array}{l} \frac{\partial N(t, z)}{\partial t} = \frac{\eta_i L_{in} S}{h\nu V} - F_P \beta \frac{N(t, z)}{\tau_{sp}} - (1 - \beta) \frac{N(t, z)}{\tau_{sp}} - \frac{N(t, z)}{\tau_{nr}} \\ \quad - v_g \sum_i (2g(t, z, \lambda) P(z) F_P)_i N_{Pi}(t, z) + D \nabla^2 N(t, z) \\ \frac{1}{v_g} \frac{\partial F_i(t, z)}{\partial t} + \frac{\partial F_i(t, z)}{\partial z} = (\Gamma g(t, z, \lambda) P(z) F_P - \alpha)_i F_i(t, z) + \frac{F_{spi}(t, z)}{L} \\ \frac{1}{v_g} \frac{\partial R_i(t, z)}{\partial t} - \frac{\partial R_i(t, z)}{\partial z} = (\Gamma g(t, z, \lambda) P(z) F_P - \alpha)_i R_i(t, z) + \frac{R_{spi}(t, z)}{L} \\ N_{Pi} \propto |F_i + R_i|^2 \end{array} \right. \quad (13)$$

here, i represents the different longitudinal modes. To keep it simple, only three main modes near to the central wavelength of the gain spectrum are simulated.

3. Simulation results and discussion

Table 1. Simulation parameters used in the model

Symbol	Parameter	Value
L	Length of active region	2×10^{-5} m
W	Width of active region	2×10^{-6} m
D	Thickness of active region	8×10^{-9} m
Γ	Optical confinement factor	0.5 [30]
Q	Quality factor	900
r_1, r_2	Mirror reflectivity	0.85
V	Cavity mode volume	$0.32 \mu\text{m}^3$
g_N	Differential gain	$3 \times 10^{-20} \text{m}^2$ [18]
N_0	Transparent carrier density	$1 \times 10^{24} \text{m}^{-3}$ [19]
α	Internal optical loss	2000m^{-1} [16]
n	Effective refractive index	3.2 [19]
ε	Gain compressive factor	$3 \times 10^{-23} \text{m}^3$ [18]
η_i	Internal quantum efficiency	0.2
β	Spontaneous emission factor	5×10^{-6} [37]
τ_{sp}	Spontaneous emission lifetime	1×10^{-9} s [32]
τ_{nr}	Non-radiative lifetime	1×10^{-9} s [32]
G_0	Parabolic gain fitting factor	$1.2 \times 10^{-9} \text{m}^{3/2}$
D	Carrier diffusion coefficient	$2 \times 10^{-4} \text{m}^2 \text{s}^{-1}$ [34]

Table 1 shows the parameters used in the simulation. The length of the FP microresonator is 20 μm which is divided into 1200 sections in the simulation. We have assumed that a quantum well active region is used in the simulation. We consider three lasing modes, including $\lambda_1 = 1.243 \mu\text{m}$ with a longitudinal mode number of $m = 104$, $\lambda_2 = 1.255 \mu\text{m}$ with $m = 103$ and $\lambda_3 = 1.267 \mu\text{m}$ with $m = 102$. The FSR between the three modes is nearly 12 nm. In the proposed experimental system, a continuous wave laser source with $\lambda = 976 \text{nm}$ is selected for interference. The incident angle is set to 51° and the required angular resolution is therefore around 1° . The spatial distribution of the vacuum field and hence the optical gain

are inherently governed by the standing waves in FP cavity with varied mode wavelengths. The mode selection can be realized by manipulating the pattern of optical injection via interference pumping. When the interference pumping along the longitudinal direction of the cavity is governed by a sinusoidal function with 103 interference nodes, which matches well with the field distribution of the central mode, the photon density and the carrier density will show the same distribution, both having 103 nodes, as shown in Figs. 2a and 2b. This spatial pumping results in the modulation in the imaginary index as shown in Fig. 2c. Fig. 2d is the spatial modulated Purcell factor of the central mode at 1.255 μm , which is corresponding to the spatial oscillation of the vacuum field in the FP-type microcavity. Figs. 2e and 2f show the spatial distributions of the carrier and photon densities for spatially modulated spontaneous emission under 0.5 mW illumination.

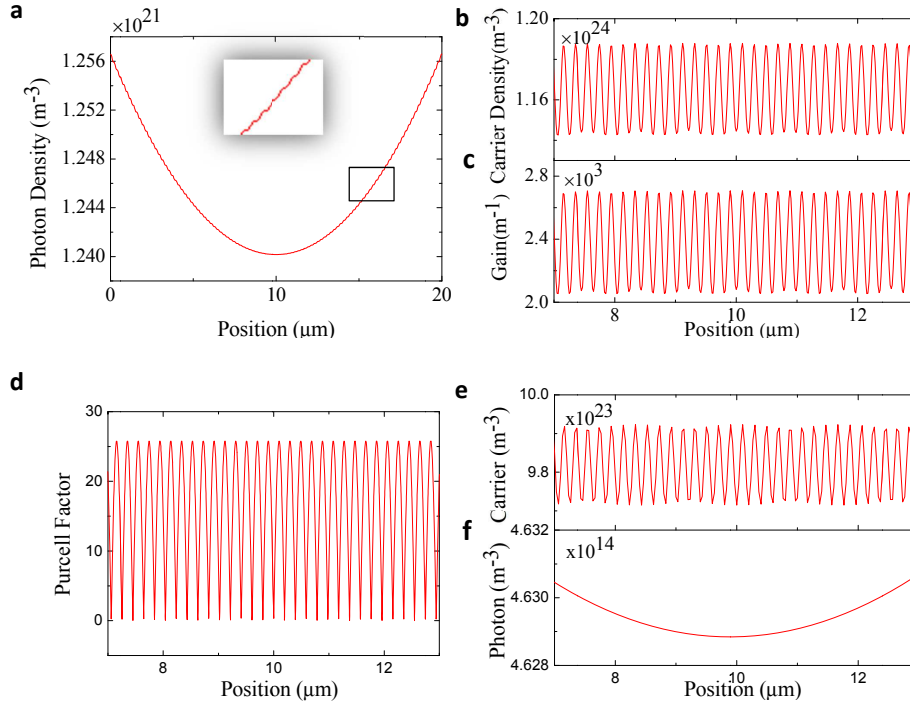


Fig. 2 The distribution of parameters along the longitudinal direction. Above threshold: **a.** Photon density distribution (the inset shows the local distribution of photon density) and **b.** Carrier density distribution under dual-beam interference with 103 interference nodes. **c.** Spatial distribution of gain under dual-beam interference with 103 interference nodes. Purcell factor: **d.** Spatial modulated Purcell factor of the central mode at 1.255 μm . Under threshold: **e.** Carrier density distribution and **f.** Photon density distribution of spatially modulated spontaneous emission under dual-beam interference with 103 interference nodes.

Owing to the interference pumping, the spatial distribution of the optical gain overlaps differently with the vacuum field of different modes, enabling effective mode selection. With uniform optical pumping, Fig. 3a shows the typical emission spectra versus pumping power. The calculated threshold is about 0.7 mW. Fig. 3b shows the spectra which has three lasing modes under 3 mW pump. The value of the SMSR at the central mode is 16.88 dB to the $\lambda_1 = 1.243 \mu\text{m}$ mode and 1.41 dB to the $\lambda_3 = 1.267 \mu\text{m}$ mode. Effectively at high pump power this becomes a dual mode laser.

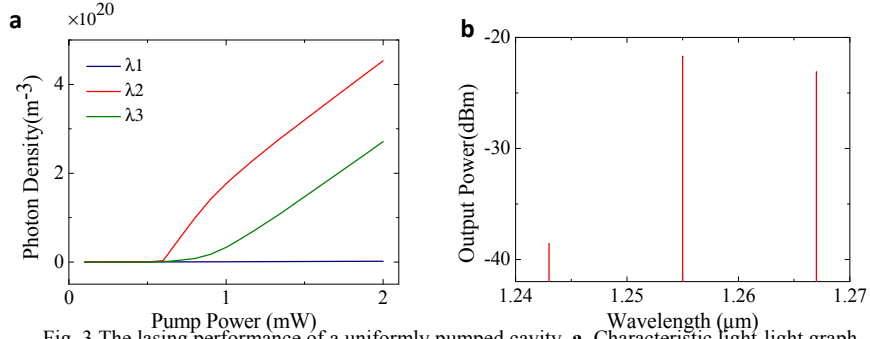


Fig. 3 The lasing performance of a uniformly pumped cavity. **a.** Characteristic light-light graph of the three lasing modes. **b.** Lasing mode spectra under uniform optical pumping.

When the interference pumping effectively overlaps with the field distribution of the central mode (CEN lines in Fig. 4), single-mode lasing is realized with a SMSR = 43.39 dB to the left mode and 40.55 dB to the right mode. Comparing with the 1.41 dB difference between modes at λ_1 and λ_2 under uniform pumping, the central mode is very effectively selected by optical interference pumping. The modified distribution of the photon density in the interference pumping case is a consequence of spatially enhanced stimulated and spontaneous emission.

Following the $m = 103$ interference pumping, we further change the number of nodes in the interference pattern to effectively overlap with the field of different modes in the longitudinal direction of the cavity. As shown in POS lines in Fig. 4, the output powers of the three modes have been altered under the $m = 102$ spatial pumping. The SMSR at the main lasing mode $\lambda_3 = 1.267 \mu\text{m}$ is 42.53 dB to λ_1 and 37.42 dB to λ_2 . The situation can be a little different under $m = 104$ interference pumping since the mode λ_1 is the weakest mode in these three lasing modes. The SMSR at λ_1 is 27.60 dB to λ_2 and 32.20 dB to λ_3 , respectively (NEG lines in Fig. 4).

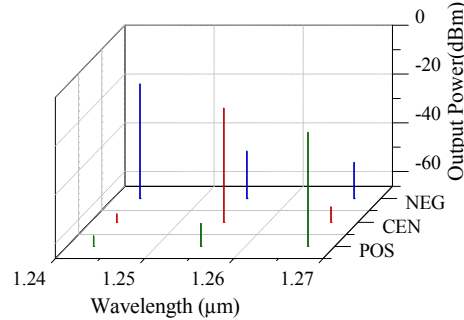


Fig. 4 The output power of three longitudinal modes using different number of interference nodes. The interference nodes of spatial pumping are 103 (CEN, red lines), 104 (NEG, blue lines), and 102 (POS, green lines), respectively.

A carrier diffusion coefficient of $2 \text{ cm}^2\text{s}^{-1}$ is used in the simulation, which is a typical value taken from the literature for InGaAsP microcavity lasers [34]. In the optical interference injection system, the carrier diffusion coefficient has a non-negligible impact on mode selection. To investigate the influence, we observe that the SMSR at the central mode $\lambda_2 = 1.255 \mu\text{m}$ reduces to 35 dB to λ_1 and 28 dB to λ_3 when the carrier diffusion coefficient increases to $10 \text{ cm}^2\text{s}^{-1}$. This degradation is attributed to reduced contrast in the spatial distribution of carriers due to the interference injection.

Comparing the characteristic light-light curves of laser cavities with uniform (Fig. 3a) and interference pumping (Fig. 5a), a clear transition from multimodal to single mode lasing is observed. A detailed comparison of the output intensity in the desired mode (λ_2) (Fig. 5b) and non-desired modes (λ_1 and λ_3) show the superior mode selection when the longitudinal profile of the pump light is effectively overlapped with the desired lasing mode. The normalized intensity of the desired mode reaches almost unity when the spatial interference pumping is above threshold. The spatially pumped cavity displays a significant growth in the value of SMSR beyond the threshold power, as shown in Fig. 5c. The value of SMSR increases with higher input power, indicating that the SMSR can be precisely controlled by changing the input. A smaller size cavity expands the FSR, revealing a higher SMSR (Fig. 5d). Applying spatial gain modulation to realise single mode lasing is suitable for microcavities with different sizes.

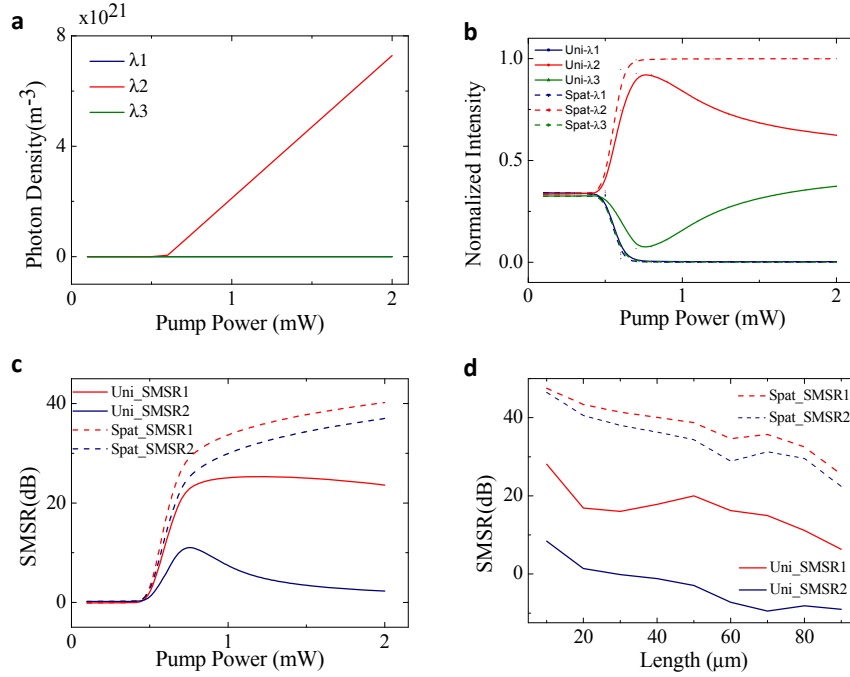


Fig. 5 Mode selection. **a.** Multi-mode light-light curve of the laser with interference pumping. The threshold power is nearly 0.7 mW. **b.** Detailed comparison of output intensity in the desired mode (λ_2) and the intensity in non-desired modes (λ_1 and λ_3), where Uni- λ_1 , Uni- λ_2 , and Uni- λ_3 denote the normalized intensity of the output under uniform pumping at the wavelength of λ_1 , λ_2 and λ_3 respectively, and Spat- λ_1 , Spat- λ_2 , and Spat- λ_3 denote the normalized intensity of the output under spatial pumping at the wavelength of λ_1 , λ_2 and λ_3 , respectively. **c.** The change of the value of SMSR from the desired mode to the non-desired modes versus input power, under uniform and spatial pumping respectively. **d.** Mode selection performance of microcavities with different sizes. Single mode lasing can be achieved in different-size cavities via gain modulation.

Both SMSR and laser performance, such as threshold pump power are related to the size of the microcavity. A smaller laser cavity expands the FSR and results in a larger mode separation, therefore a higher SMSR can be obtained. In the simulation, we have kept the same pumping density for uniformly and nonuniformly pumped microcavities. This proves that the SMSR is improved under nonuniform injection compared to a cavity with uniform injection.

Fig 6 shows the time evolution of the carrier density (Fig. 6a) and photon density of the central mode (Fig. 6b) in uniformly and spatially pumped cavities, respectively. The turn-on

delay is an important parameter for semiconductor lasers and extensive studies have indicated that the delay time is principally determined by the carrier dynamics [37, 38]. The simulation results indicate that there is a shorter turn-on delay for the spatially pumped cavity, in which the interference injection interacts with the vacuum field distribution. This affects the carrier dynamics and hence increases the non-radiative electron scattering rates. However, the decrease of the turn-on delay time in our system is relatively small. This is due to the slight differences in the threshold carrier density under uniform and spatial optical pumping, which directly affect the carrier recombination rate. Moreover, the damping rate of the turn-on process is modified by changes to the spontaneous emission process caused by spatial pumping

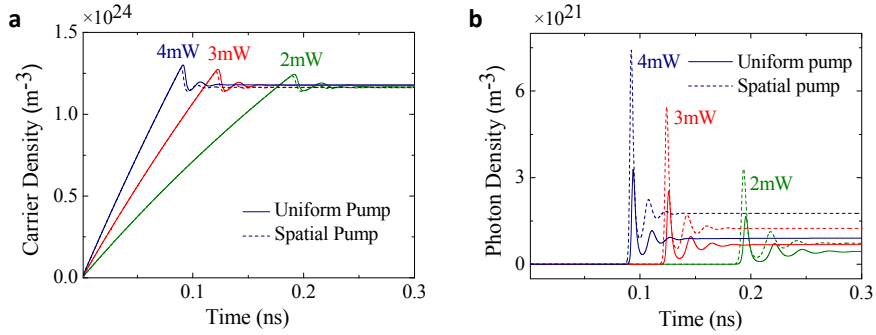


Fig. 6 Turn-on delay of uniformly and spatially pumped cavities with different pumping power. **a.** Turn-on delay dynamics of carriers. **b.** Turn-on delay dynamics of photon density of the central mode.

We have calculated the small signal response [39-41] of both the uniformly and spatially pumped microcavity lasers based on the extended rate equation model. The results are shown in Fig. 7. Clear relaxation resonances are observed for injected light powers ranging from 3 mW to 48 mW. The corresponding 3 dB bandwidth varies from 4.7 to 15.1 GHz for the uniformly pumped cavity (Fig. 7a solid lines) and 6.2 to 21.3 GHz for the spatially pumped cavity (Fig. 7a dotted lines), respectively. Focusing on the change of modulation response amplitude, the damping factor is decreased in the spatially pumped case. We plot the 3 dB linewidth versus the square root of light power minus threshold light power (Fig. 7b). The proportional constant is 2.23 GHz mW^{-0.5} for the uniformly pumped cavity, but the modulation efficiency increased to 3.70 GHz mW^{-0.5} for the spatially pumped cavity. The higher-speed performance is achieved due to an immediate interaction between non-uniform carrier injection with optical interference pumping and the vacuum field of the standing wave.

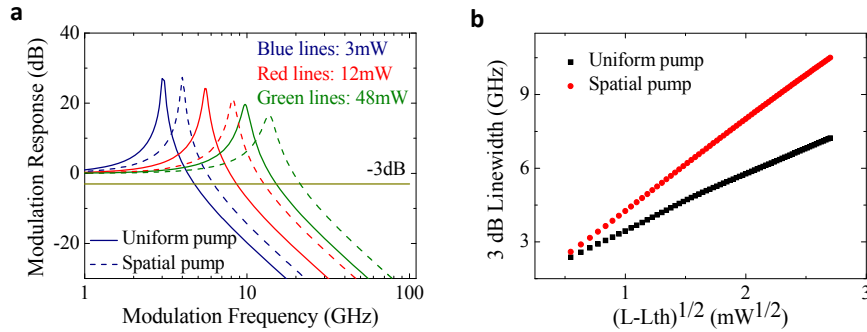


Fig. 7 Small signal responses of the microcavity lasers. **a.** Small signal responses of the uniformly and spatially pumped cavities under varying light injection. **b.** 3 dB linewidth as a

function of the light power $(L-L_{th})^{1/2}$, the modulation efficiency of spatial pumping is increased comparing to the uniform pumping.

4. Conclusions

In conclusion, we have proposed an extended rate equation model which considers the interplay between the vacuum electromagnetic field of standing waves and external optical injection via laser interference. Simulation results show that the lasing mode can be effectively selected (with a SMSR over 40 dB) when the longitudinal profile of the pumping light effectively overlaps that of the field distribution of the desired lasing mode. This mode selection mechanism shows that the value of SMSRs can be precisely controlled by altering the input and that the model can be applied to micro-resonators with different sizes and shapes, such as FP and whispering-gallery-mode resonators [42]. Moreover, a shorter turn-on delay and higher-speed modulation can be possible using optical interference pumping compared to uniformly pumped lasers. This model has been used to explore the performance of micro- and nano-resonators through a combination of a classical model of multimode competition in semiconductor lasers and a quantum-optics understanding of radiative processes in microcavities.

Funding

Natural National Science Foundation of China (NSFC) (61574138, 61974131, 61905217).
Engineering and Physical Sciences Research Council (EPSRC) (EP/P020399).
Natural Science Foundation of Zhejiang Province (LQ19F040010).

Disclosures

The authors declare no conflicts of interest.

References

1. H. J. Caulfield and S. Dolev, "Why future supercomputing requires optics," *Nat. Photonics* **4**(5), 261–263 (2010).
2. H. Zhu, Y. Fu, F. Meng, X. Wu, Z. Gong, Q. Ding, M. V. Gustafsson, M. T. Trinh, S. Jin, and X. Y. Zhu, "Lead halide perovskite nanowire lasers with low lasing thresholds and high quality factors," *Nat. Mater.* **14**(6), 636–642 (2015).
3. M. Asada, A. Kameyama, and Y. Suematsu, "Gain and intervalence band absorption in quantum-well lasers," *IEEE J. Quantum Electron.* **20**(7), 745-753 (1984).
4. L. Feng, Z. J. Wong, R. M. Ma, Y. Wang, and X. Zhang, "Single-mode laser by parity-time symmetry breaking," *Science* **346**(6212), 972-975 (2014).
5. H. Hodaei, M. A. Miri, M. Heinrich, D. N. Christodoulides, and M. Khajavikhan, "Parity-time-symmetric microring lasers," *Science* **346**(6212), 975-978 (2014).
6. Z. Ren, Q. Kan, G. Ran, C. Jin, L. Yuan, X. Wang, L. Tao, H. Yu, L. Zhang, W. Chen, K. He, R. M. Ma, J. Pan, and W. Wang, "Hybrid single-mode laser based on graphene Bragg gratings on silicon," *Opt. Lett.* **42**(11), 2134-2137 (2017).
7. S. Jung, A. Jiang, Y. Jiang, K. Vijayraghavan, X. Wang, M. Troccoli, and M. A. Belkin, "Broadly tunable monolithic room-temperature terahertz quantum cascade laser sources," *Nat. Commun.* **5**, 4267 (2014).
8. H. Altug, D. Englund, and J. Vučković, "Ultrafast photonic crystal nanocavity laser," *Nat. Phys.* **2**(7), 484-488 (2006).
9. Y. Luo, Y. Nakano, K. Tada, T. Inoue, H. Hosomatsu, and H. Iwaoka, "Purely gain - coupled distributed feedback semiconductor lasers," *Appl. Phys. Lett.* **56**(17), 1620-1622 (1990).
10. K. David, G. Morthier, P. Vankwikelberge, R. G. Baets, T. Wolf, and B. Borchert, "Gain-coupled DFB lasers versus index-coupled and phase shifted DFB lasers: a comparison based on spatial hole burning corrected yield," *IEEE J. Quantum Electron.* **27**(6), 1714-1723 (1991).
11. A. J. Lowery and D. Novak, "Performance comparison of gain-coupled and index-coupled DFB semiconductor lasers," *IEEE J. Quantum Electron.* **30**(9), 2051-2063 (1994).
12. F. Gu, F. Xie, X. Lin, S. Linghu, W. Fang, H. Zeng, L. Tong, and S. Zhuang, "Single whispering-gallery mode lasing in polymer bottle microresonators via spatial pump engineering," *Light Sci. Appl.* **6**(10), e17061 (2017).

13. C. Fernandez-Oto, G. J. de Valcárcel, M. Tlidi, K. Panajotov, and K. Staliunas, "Phase-bistable patterns and cavity solitons induced by spatially periodic injection into vertical-cavity surface-emitting lasers," *Phys. Rev. A* **89**(5), 055802 (2014).
14. R. S. Tucker, "High-speed modulation of semiconductor lasers," *J. Lightwave Technol.* **3**(6), 1180–1192 (1985).
15. D. Wang, Z. Wang, Z. Zhang, Y. Yue, D. Li, and C. Maple, "Effects of polarization on four-beam laser interference lithography," *Appl. Phys. Lett.* **102**(8), 081903 (2013).
16. C. Y. Jin, Y. Z. Huang, L. J. Yu, and S. L. Deng, "Detailed model and investigation of gain saturation and carrier spatial hole burning for a semiconductor optical amplifier with gain clamping by a vertical laser field," *IEEE J. Quantum Electron.* **40**(5), 513-518 (2004).
17. C. Y. Jin, Y. Z. Huang, L. J. Yu, and S. L. Deng, "Detailed model and investigation of gain saturation and carrier spatial hole burning for a semiconductor optical amplifier with gain clamping by a vertical laser field," *IEEE J. Quantum Electron.* **40**(5), 513-518 (2004).
18. L. M. Zhang, S. F. Yu, M. C. Nowell, D. D. Marcenac, J. E. Carroll, and R. G. S. Plumb, "Dynamics analysis of radiation and side mode suppression in a 2nd-order DFB laser using time-domain laser signal traveling wave model," *IEEE J. Quantum Electron.* **30**(6), 1389-1395 (1994).
19. L. Wei, H. Wei-Ping, and L. Xun, "Digital filter approach for Simulation of a complex integrated laser diode based on the traveling-wave model," *IEEE J. Quantum Electron.* **40**(5), 473-480 (2004).
20. D. Lei, Z. Ruikang, W. Dingli, Z. Shengzhi, J. Shan, Y. Yonglin, and L. Shuihua, "Modeling Widely Tunable Sampled-Grating DBR Lasers Using Traveling-Wave Model With Digital Filter Approach," *J. Lightwave Technol.* **27**(15), 3181-3188 (2009).
21. M. Djiango, T. Kobayashi, and W. J. Blau, "Cavity-enhanced stimulated emission cross section in polymer microlasers," *Appl. Phys. Lett.* **93**(14), 3 (2008).
22. A. J. Campillo, J. D. Eversole, and H. B. Lin, "Cavity quantum electrodynamic enhancement of stimulated emission in microdroplets," *Phys. Rev. Lett.* **67**(4), 437-440 (1991).
23. B. Romeira and A. Fiore, "Purcell Effect in the Stimulated and Spontaneous Emission Rates of Nanoscale Semiconductor Lasers," *IEEE J. Quantum Electron.* **54**(2), 1-12 (2018).
24. W. Wei, X. Zhang, X. Yan, and X. Ren, "Observation of enhanced spontaneous and stimulated emission of GaAs/AlGaAs nanowire via the Purcell effect," *AIP Advances.* **5**(8), 087148 (2015).
25. N. Gregersen, T. Suhr, M. Lorke, and J. Mørk, "Quantum-dot nano-cavity lasers with Purcell-enhanced stimulated emission," *Applied Physics Letters* **100**(2012).
26. M. Lorke, T. Suhr, N. Gregersen, and J. Mørk, "Theory of nanolaser devices: Rate equation analysis versus microscopic theory," *Phys. Rev. B.* **87**(20), 205310 (2013).
27. P. A. M. Dirac, "The quantum theory of the emission and absorption of radiation," *Proc. R. soc. Lond. Ser. A-Contain. Pap. Math. Phys. Character* **114**(767), 243-265 (1927).
28. E. Fermi, "High energy nuclear events," *Prog. Theor. Phys.* **5**(4), 570-583 (1950).
29. E. M. Purcell, "Spontaneous emission probabilities at radio frequencies," *Phys. Rev.* **69**(11-1), 681-681 (1946).
30. T. P. Lee, C. A. Burrus, J. A. Copeland, A. G. Dentai, and D. Marcuse, "Short-cavity InGaAsP injection lasers-dependence of mode spectra and single longitudinal mode power on cavity length," *IEEE J. Quantum Electron.* **18**(7), 1101-1113 (1982).
31. T. Suhr, N. Gregersen, K. Yvind, and J. Mørk, "Modulation response of nanoLEDs and nanolasers exploiting Purcell enhanced spontaneous emission," *Opt. Express* **18**(11), 11230-11241 (2010).
32. E. K. Lau, A. Lakhani, R. S. Tucker, and M. C. Wu, "Enhanced modulation bandwidth of nanocavity light emitting devices," *Opt. Express* **17**(10), 7790-7799 (2009).
33. D. X. Zhu, S. Dubovitsky, W. H. Steier, J. Burger, D. Tishinin, K. Uppal, and P. D. Dapkus, "Ambipolar diffusion coefficient and carrier lifetime in a compressively strained InGaAsP multiple quantum well device," *Appl. Phys. Lett.* **71**(5), 647-649 (1997).
34. K. Nozaki and T. Baba, "Carrier and photon analyses of photonic microlasers by two-dimensional rate equations," *IEEE J. Sel. Area. Commun.* **23**(7), 1411–1417 (2005).
35. R. Olshansky, P. Hill, V. Lanzisera, and W. Powazinik, "Frequency response of 1.3um InGaAsP high speed semiconductor laser," *IEEE J. Quantum Electron.* **23**(9), 1410-1418 (1987).
36. M. J. Adams and M. Osinski, "Longitudinal mode competition in semiconductor lasers-rate equations revisited," *IEE Proceedings-I Communications Speech and Vision* **129**, 271-274 (1982).
37. K. Lüdge, M. J. P. Bormann, E. Malić, P. Hövel, M. Kuntz, D. Bimberg, A. Knorr, and E. Schöll, "Turn-on dynamics and modulation response in semiconductor quantum dot lasers," *Phys. Rev. B.* **78**(3), 035316(2008).
38. H. Deng, G. Weihs, C. Santori, J. Bloch, and Y. Yamamoto, "Condensation of semiconductor microcavity exciton polaritons," *Science* **298**(199), 199-202 (2002).
39. K. Kamath, J. Phillips, H. Jiang, J. Singh, and P. Bhattacharya, "Small-signal modulation and differential gain of single-mode self-organized In_{0.4}Ga_{0.6}As/GaAs quantum dot lasers," *Appl. Phys. Lett.* **70**(22), 2952-2953 (1997).
40. C. Wang, F. Grillot, and J. Even, "Impacts of Wetting Layer and Excited State on the Modulation Response of Quantum-Dot Lasers," *IEEE J. Quantum Electron.* **48**(9), 1144-1150 (2012).
41. K. Takeda, T. Sato, A. Shinya, K. Nozaki, W. Kobayashi, H. Taniyama, M. Notomi, K. Hasebe, T. Kakitsuka, and S. Matsuo, "Few-fJ/bit data transmissions using directly modulated lambda-scale embedded active region photonic-crystal lasers," *Nat. Photonics.* **7**(7), 569-575 (2013).

42. W. H. Guo, Y. Z. Huang, Q. Y. Lu, and L. J. Yu, "Modes in square resonators," *IEEE J. Quantum Electron.* **39**(12), 1563-1566 (2003).